Heat and Mass Transfer 34 (1998) 247–254 © Springer-Verlag 1998

Heat transfer in open cell polyurethane foam insulation

J.-W. Wu, H.-S. Chu

Abstract This paper study systematic investigates the combined conductive and non-gray radiative heat transfer of open cell polyurethane (PU) foam in the pressure range between 760 and 0.02 Torr. Direct transmission measurements are also taken using Fourier transform infrared (FTIR) spectrometer. In doing so, experimental results are obtained for the spectral extinction coefficient from 2.5 to 25 μm. In addition, the P-3 approximation method along with the box model is employed to calculate the non-gray radiative heat flux. The diffusion approximation method is also applied to calculated the radiative conductivity. Also tested herein are three samples with different cell sizes ranging from 330 to 147 μm. According to those results, the spectral extinction coefficient increases with a decrease of cell size, leading to a decrease of thermal conductivity. Moreover, evacuating the gases in the foam cells can reduce the thermal conductivity of the PU foam by as much as 75%. Furthermore, radiative heat transfer accounts for about 4% of total heat transfer at 760 Torr and increases to 20% at 0.02 Torr.

List of symbols

f_v solid volume fraction
$I_{b\lambda}$ spectral blackbody intensity, [W/(m^{2}μm)]
k_c solid conductivity, [W/mK]
k_r radiative conductivity, [W/mK]
L thickness of the medium, [m]
q^c conductive heat flux, [W/m^2]
q^r radiative heat flux, [W/m^2]
q^t total heat flux, [W/m^2]
$T_{1,2}$ temperature of hot wall & cold wall, [K]
x coordinate

Greek symbols

λ wavelength, [μm]
$\varepsilon_{1,2}$ wall emissivity
κ_λ extinction coefficient, [m^{-1}]
ψ_0 incident radiation
ψ_1 radiative heat flux
ψ_2 second moment of incident radiation
ψ_3 third moment of incident radiation
σ Stefan-Boltzmann constant, 5.667×10^{-3}[W/(m^{2}K^4)]

Subscripts

b blackbody
c conductive
r radiative
1,2 hot wall and cold wall

1 Introduction

Rigid polyurethane foam, consisting of a highly porous but solid body with a cellular structure, has found diverse applications: from buildings to refrigerators. Heat transport occurs via gaseous and solid thermal conduction as well as radiation. Radiative heat transfer profoundly influences the design of many engineering systems, particularly in predicting the heat transfer rates through an absorbing, emitting, and scattering material. However, realistic predictions, even in extremely simple geometrical systems, are difficult to obtain owing to the frequency and temperature dependent radiative properties of the media.

Thermal insulation has received extensive interest in recent decades. Aronson et al. [1] estimated the absorption and scattering coefficients using the geometrical optics theory and the Rayleigh approximation by separately considering coarse and fine fibers. In a related work, Tong and Tien [2] demonstrated extent to which thermal radiation influences in fibrous insulation. That investigation also reviewed the analytical models capable of predicting radiative heat transfer in fibrous media based on a simple conductive and more elaborate radiative approach. Later, Tong and Tien [3] and Tong et al. [4] analytically and experimentally studied radiative heat transfer in lightweight fibrous insulation. In their investigations, two-flux and linear anisotropic scattering models were used to predict the radiant heat flux; the radiative properties of fibrous insulation were calculated as well. For this purpose, they examined the radiative heat transfer in this anisotropically scattering material using an infrared spectrophotometer and a guarded hot-plate apparatus.

Received on 20 April 1998

J.-W. Wu, H.-S. Chu
Department Mechanical Engineering
National Chiao Tung University
Hsinchu, Taiwan, Republic of China

Correspondence to: H.-S. Chu

The authors would like to thank the National Science Council of the Republic of China for financially supporting this research under Contract No. NSC86-2221-E-009-047. The National Center for High-Performance Computing (NCHC) is appreciated for performing the numerical calculations.

Another method attempts to reduce gas conduction through the porous insulation by use of ultra-fine powders with diameters of the order of 10 nm. In pioneering work, Scheuerpflug et al. [5] investigated the consolidated ultra-fine powder insulation in the form of rigid S_iO_2-aerogel tiles for double-plane window application. Chu et al. [6] systematically studied, for the first time, the spectral radiation heat transfer through the ultra-fine powder insulation Aerosil 380 with particle diameters close to 7 nm. Gas conduction, which is characterized by the molecular mean free path, can be significantly reduced if the pore size between solid particles is less than the mean free path. In a related work, Heinemann et al. [7] theoretically and experimentally investigated the thermal transport in low density silica aerogel over a wide range of optical thickness and ratio of radiative to conductive heat transfer. That investigation also proposed a high precision numerical method to calculate the temperature profile and the total heat flux in these semi-transparent, non-scattering, non-gray media.

The heat transfer modes in polyurethane foams are determined by gaseous conduction within the pores, conduction via the solid structures of the foams, and by radiative transfer. Among the related numerical and experimental studies: Glicksman et al. [8] concentrated on the radiative contribution towards heat transfer in foam. Foams scatter radiation due to the interaction of the radiation with struts and walls such that radiative transfer can be modeled as a diffusion process. Kuhn et al. [9] thoroughly investigated polystyrene (PS) and a polyurethane (PU) foams and the contribution of each thermal transfer modes. In particular, they theoretically and experimentally studied radiative transfer. In a similar work, Doermann and Sacadura [10] presented a predictive model for thermal transfer in open-cell foam insulation as a function of foam morphology, porosity, thermal properties of solid and gaseous phases, and optical properties of the solid phase. Caps et al. [11] recently measured the thermal conductivity of polyimide foams in the temperature range of 173–323 K under different gas pressures and using different gas types (CO_2 and Ar). Their investigation also developed a quantitative model to accurately predict the thermal conductivity of polyimide foam as a function of density, gas pressure and temperature. Hahn et al. [12] presented a model to calculate the transient combined radiative/conductive heat transfer in heterogeneous semi-transparent materials at elevated temperatures. Those investigators also applied the three flux model to solve the integrol-differential equation for an 8-band-simulation. Tseng et al. [13] more recently investigated the thermal conductivity of polyurethane foam in the temperature range between 300 and 20 K for the development of liquid hydrogen storage tanks. In general, heat transfer occurs in foam by natural convection, gas conduction, solid-solid conduction and radiation. In addition, the dominant heat transfer modes in foam insulation are thermal radiation and solid-solid conduction if the foam insulation systems are evacuated. Moreover, a low apparent thermal conductivity can be achieved in an evacuated volume because the gas conductive and convective heat transfer modes do not exist in a vacuum.

This study investigates the heat transfer of evacuated open cell polyurethane foam with the cell size ranging from 330 to 147 μm. This study focuses primarily on determining the heat transfer mode in this system and predicting the radiative thermal conductivity. A Fourier transform infrared spectrometer is experimentally used to measure the spectral extinction coefficient in the wavelength range of 2.5 to 25 μm. In addition, effective thermal conductivity is measured with a guarded-hot-plate system. The albedo developed by Kuhn et al. [9] is employed for the analysis. The stepwise gray or box model [14] is also applied to incorporate the effects of the non-gray characteristics. Moreover, the radiative heat transfer is calculated using the P-3 approximation, which has been demonstrated to effectively generate accurate approximate solutions to the gray problem [15].

2 Theoretical analysis

Consider a non-gray absorbing, emitting and isotropically scattering polyurethane foam that transfers energy through parallel plates as depicted in Fig. 1. Both plates have the same wall emissivity and are maintained constant at different wall temperature. The left bounding plate is hotter than that of the right one. The physical properties of the foam are assumed to be independent of temperature, particularly the evacuated solid thermal conductivity. Under these conditions, the energy equation can be expressed as

$$k_c \frac{d^2T}{dx^2} - \frac{dq^r}{dx} = 0 \tag{1}$$

associated with the following boundary conditions:

$$T(0) = T_1, \quad T(L) = T_2, \tag{2}$$

The radiative heat flux q^r can be obtained by integrating of radiative intensity I, which can be determined by solving the equation of transfer. Herein, the P-3 approximation is used to calculate radiative heat transfer. The spectral equations for the P-3 approximation [16] can be written as:

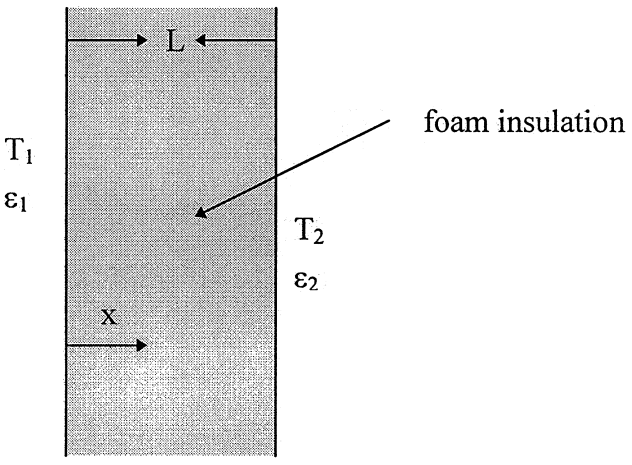

Fig. 1. Physical model and coordinate system

$$\frac{d\psi_{0\lambda}}{dx} = -3\kappa_\lambda(1-\omega f_1)\psi_{1\lambda} + \frac{14}{3}\kappa_\lambda(1-\omega f_3)\psi_{3\lambda} \ , \tag{3a}$$

$$\frac{d\psi_{1\lambda}}{dx} = 4\pi\kappa_\lambda(1-\omega)I_{b\lambda} - \kappa_\lambda(1-\omega f_0)\psi_{0\lambda} \ , \tag{3b}$$

$$\frac{d\psi_{2\lambda}}{dx} = -\frac{7}{3}(1-\omega f_3)\psi_{3\lambda} \ , \tag{3c}$$

$$\frac{d\psi_{3\lambda}}{dx} = -\frac{8}{3}\pi(1-\omega)I_{b\lambda} + \frac{2}{3}(1-\omega f_0)\psi_{0\lambda} - \frac{5}{3}(1-\omega f_2)\psi_{2\lambda} \ , \tag{3d}$$

where the value of $f_{1,2,3}$ depend on the type of scattering being modeled and by definition, $\psi_0(x)$ and $\psi_1(x)$ denoted the incident radiation and the radiative heat flux, respectively. In addition, $\psi_2(x)$ and $\psi_3(x)$ represent the second and third moment of incident radiation respectively. Moreover, $I_{b\lambda}$ is the blackbody intensity. The boundary conditions for Eqs. (3a) to (3d) are

at $x = 0$,

$$\varepsilon_1\psi_{0\lambda} + 2(2-\varepsilon_1)\psi_{1\lambda} + \frac{5}{4}\varepsilon_1\psi_{2\lambda} = 4\pi\varepsilon_1 I_{b\lambda},$$

$$\varepsilon_1\psi_{0\lambda} + \frac{12}{5}(2-\varepsilon_1)\psi_{1\lambda} + \frac{5}{2}\varepsilon_1\psi_{2\lambda} + \frac{8}{5}(2-\varepsilon_1)\psi_{3\lambda} = 4\pi\varepsilon_1 I_{b\lambda} \ , \tag{4a}$$

at $x = L$,

$$\varepsilon_2\psi_{0\lambda} - 2(2-\varepsilon_2)\psi_{1\lambda} + \frac{5}{4}\varepsilon_2\psi_{2\lambda} = 4\pi\varepsilon_2 I_{b\lambda},$$

$$\varepsilon_2\psi_{0\lambda} - \frac{12}{5}(2-\varepsilon_2)\psi_{1\lambda} + \frac{5}{2}\varepsilon_2\psi_{2\lambda} - \frac{8}{5}(2-\varepsilon_2)\psi_{3\lambda} = 4\pi\varepsilon_2 I_{b\lambda} \ , \tag{4b}$$

where $\varepsilon_{1,2}$ denotes the hemispherical emissivity at the wall for $x = 0$, and $x = L$, respectively. Simultaneously solving Eqs. (3a)–(3d) using the BVPFD subroutine of a commercially available software package called IMSL allows us to obtain the incident radiation $\psi_{0\lambda}$ deemed necessary for the energy equation and the radiative heat flux q^r requisite for heat-transfer evaluation. Herein, P-3 approximation is applied to non-gray radiation, by dividing the participating bands into a number of subbands. The extinction coefficient of each subband is assumed to remain constant, as solved by using box model. By using the radiation intensity calculated in Eqs. (3a)–(3d), the derivative of the radiative heat flux can be written as

$$\nabla \cdot q^r = \sum_{i=1}^{N} \kappa_{\lambda i}[4\pi(1-\omega)I_{b\lambda i} - (1-\omega f_0)\psi_{0\lambda i}] \cdot \tag{5}$$

The total heat flux across the PU foam is calculated from

$$q^t = -k_c\frac{dT}{dx} - k_r\frac{dT}{dx} \tag{6}$$

where k_r represents the radiative thermal conductivity

Equations (1), (3a–3d) and (5) are solved using the finite-difference method to determine the radiative heat flux and temperature distribution. The solution procedure is outlined as follows:

1. Guess the temperature and intensity distributions;
2. Solve the energy equation by a point-by-point iterative method to obtain a new temperature distribution. The conductive heat flux can be obtained from the temperature distribution;
3. With the guessed intensity fields and the new temperature, solve the spectral equations to obtain the new intensity distribution and radiative heat flux; and
4. Repeat steps (2) and (3), until the convergence criterion for heat flux on each point is satisfied.

The convergence criterion for all calculations is set at

$$\left|T_i^{new} - T_i^{old}\right| \le 1 \times 10^{-7} \tag{7}$$

to satisfy all mesh points. This iterative procedure is continued until the convergence criterion is reached.

3
Extinction coefficient measurement

Samples with cell sizes of 330, 214 and 147 μm are marked as "sample A", "sample B", and "sample C", respectively. In this study, the direct transmission measurements are taken in the wavelength range from 2.5 to 25 μm using a Fourier transform infrared spectrometer (Perkin-Elmer Spectrum 2000). Each sample is measured after removing the moisture effects. In addition, transmission data are used to calculate the spectral extinction coefficient κ_λ, according to Beer's law, $I_\lambda(x)/I_{0\lambda} = \exp(-\kappa_\lambda x)$. Figure 2 presents the extinction coefficients κ_λ of samples A, B, and C. According to this figure, the extinction coefficient increases with a decrease of the cell size.

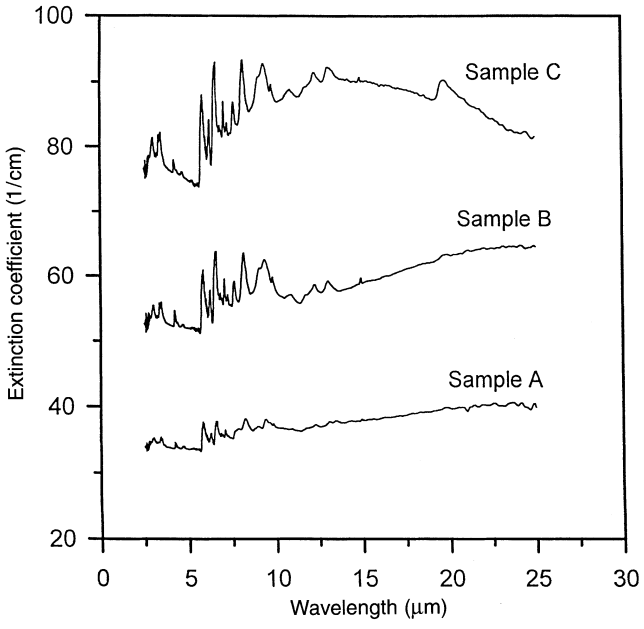

Fig. 2. Specific absorption coefficient for three different cell sizes

4 Results and discussion

This study verifies the influence of grid size on the numerical results by performing a grid-independence test for five different grid sizes. Table 1 summarizes the results of temperature, heat fluxes (at middle plane) and cpu time. This table reveals that the temperature and heat fluxes only slightly differ between grids 51 and 71. Hereinafter, the uniform grid system of 51 is selected for all the calculations. Next, an attempt is made to demonstrate that the number of spectral bands much represent the spectral variation of extinction coefficient with sufficient accuracy. Table 2 compares the temperature and heat fluxes (at middle plane) results for different band numbers. According to this table, variations in temperature and heat flux are only slight when the band number exceeds 30. Therefore, thirty bands of extinction coefficients between 2.5 to 25 μm are used to calculate the non-gray radiation heat transfer, as described in the following.

Table 3 displays the effective thermal conductivities of three samples measured by a guarded-hot-plate system. The fact that the radiative conductivity is independent of evacuation pressure allows us to obtain the conductive conductivity by substracting the radiative conductivity from measured effective thermal conductivity. In addition, according to our results, the variation of effective thermal conductivity becomes only slight when the pressure falls below than 0.02 Torr. Hence, the gaseous heat transfer can be reasonably neglected when the evacuation pressure is 0.02 Torr. To produce the sample in this study, the foam is put into the laminated film bag and was evacuated to low pressure of 0.02 Torr. Figure 3 illustrates how cell size influences the heat flux at $T_1 = 301$ K, $T_2 = 271$ K, $\varepsilon_1 = 0.1$, $\varepsilon_2 = 0.1$, $L = 0.01$ m, and at an evacuation pressure of 0.02 Torr. The differences in cell size are attributed to the influence of the open cell walls and the struts having formed at the junctions of the cell walls. Such an influence is owing to that the extinction coefficient decreases with an increase of the cell size; the radiative heat flux increases with an increase of cell size as well. According to our results, the conductive heat flux also exhibits the same trend.

Table 4 compares the radiative and conductive heat fluxes (at mid-plane) for three samples at evacuation pressures ranging from 760 to 0.02 Torr. As expected, the radiative heat fluxes only negligibly differ for the different pressure conditions of the three samples were small. This table also reveals that the conductive heat flux of sample A at 760 Torr is around five times larger than that at evacuation pressure 0.02 Torr. Based on above results, we can conclude that gaseous heat transfer is the dominant heat transfer mode at atmospheric condition. As mentioned earlier the gaseous heat transfer can be reasonable ne-

Table 1. Comparison of the results for different grid sizes of sample A at $x = 0.005$ m

Grid no.	Temp. (K)	q^r (W/m^2)	q^c (W/m^2)	Cpu time (min.)
31	286.318	5.2359	22.6932	11.31
51	286.301	5.2108	22.5890	42.07
71	286.288	5.2032	22.5853	91.73
91	286.243	5.1980	22.5487	124.87
111	286.251	5.1965	22.5401	227.84

Table 2. Comparison of the results for different band numbers of sample A at $x = 0.005$ m

Band no.	Temp. (K)	q^r (W/m^2)	q^c (W/m^2)
10	286.30	5.1943	22.5901
20	286.30	5.2062	22.5786
30	286.30	5.2108	22.5890
40	286.29	5.2118	22.5907
50	286.30	5.2102	22.5786

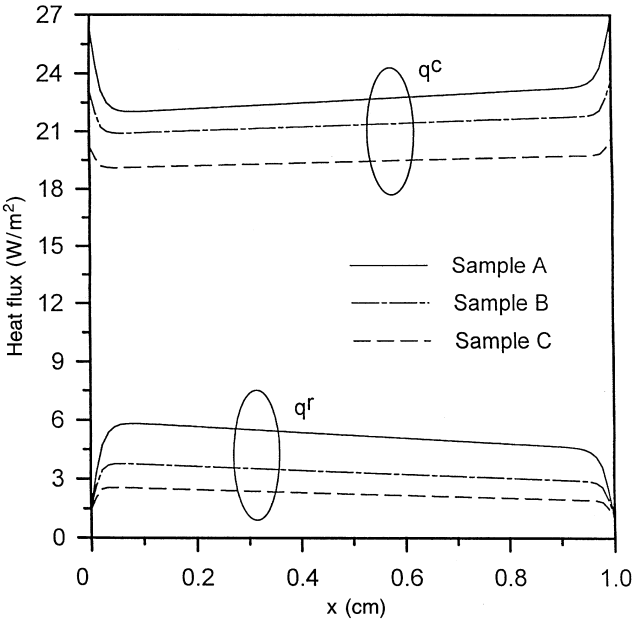

Fig. 3. Effects of cell-size on heat flux for three different cell sizes with $T_1 = 301$ K, $T_2 = 271$ K, $\varepsilon_1 = 0.1$, $\varepsilon_2 = 0.1$, $L = 0.01$ m, and an evacuation pressure of 0.02 Torr

Table 3. Summary of experimental data for three different samples at $T_m = 286$ K

Parameter	Sample	A	B	C
f_v		0.037	0.038	0.042
Cell size (μm)		330	214	147
760 Torr	k_{eff} (mW/mK)	34.2	33.87	33.4
9 Torr	k_{eff} (mW/mK)	33.4	32.5	31.3
1 Torr	k_{eff} (mW/mK)	23.5	24.94	13.9
0.1 Torr	k_{eff} (mW/mK)	22	16.7	12.7
0.02 Torr	k_{eff} (mW/mK)	9.5	8.35	7.3
0.014 Torr	k_{eff} (mW/mK)	9.4	8.2	7.2

glected when the evacuation pressure is 0.02 Torr. In addition, the conduction contribution can be regarded as solid conduction only at 0.02 Torr. The relative contributions of solid, gaseous and radiative modes to the total heat transfer at evacuation pressure 760 Torr can be predicted to be 22.2%, 72.6% and 5.2%, respectively. With a decreasing pressure, the radiative contribution increases and contributes about 18.7% of the total heat transfer when the pressure is 0.02 Torr. Table 5 compares the values of the radiative and conductive heat fluxes (at middle-plane) for three different samples with different mean temperatures at an evacuation pressure of 0.02 Torr. In general, radiative heat transfer becomes even more critical at higher temperatures. By raising the mean temperature from 260 to 356 K, an increase in the radiative contribution to total heat transfer in sample A is raised from 14.2% to 31.9%. When the mean temperature is fixed, the relative radiative contribution increases with an increase of cell size. Table 6 compares the effects of thickness on the values of radiative and conductive heat fluxes (at middle-plane) for three samples. This table also reveals that heat fluxes linearly decrease with an increase of thickness.

Figure 4 illustrates the effects of evacuation pressure on radiative heat flux for sample A and C. For the gray radiative heat transfer, the extinction coefficient is taken as one band averaged value by the box model. The values of extinction coefficient for sample A and sample C are 3757.98 m^{-1} and 8585.37 m^{-1}, respectively. At an evacuation pressure of 760 and 0.02 Torr, the gray and non-gray methods appear to significantly differ because the gains in radiant energy due to radiation emitted by the gray medium are larger than those of the non-gray one. For simplicity, foam is usually considered a gray body with a constant value of extinction coefficient over all wavelength. In this case, the gray radiation method overestimates the

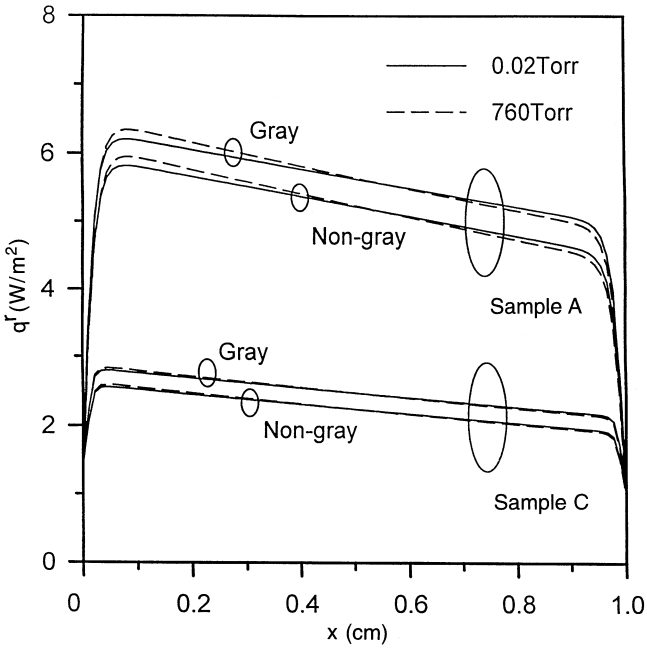

Fig. 4. Effects of evacuation pressure on radiative heat flux with $T_1 = 301$ K, $T_2 = 271$ K, $\varepsilon_1 = 0.1$, $\varepsilon_2 = 0.1$, and $L = 0.01$ m

Table 4. Comparison of the heat fluxes in three different samples at $x = 0.005$ m

Pressure (Torr)	Sample A		Sample B		Sample C	
	q^r (W/m^2)	q^c (W/m^2)	q^r (W/m^2)	q^c (W/m^2)	q^r (W/m^2)	q^c (W/m^2)
760	5.2268	96.6616	3.3244	97.9124	2.2378	97.7634
9	5.2264	94.2523	3.3244	94.0843	2.2378	91.4619
1	5.2251	64.5697	3.3244	71.1156	2.2401	39.2693
0.1	5.2249	60.0744	3.3243	46.4067	2.2400	35.6621
0.02	5.2103	22.5872	3.3236	21.3495	2.2429	19.4634

Table 5. Comparison of the heat fluxes in three different samples at $x = 0.005$ m

T_m (K)	Sample A		Sample B		Sample C	
	q^r (W/m^2)	q^c (W/m^2)	q^r (W/m^2)	q^c (W/m^2)	q^r (W/m^2)	q^c (W/m^2)
260	3.4470	20.5825	2.1743	19.3759	1.4655	17.6471
286	5.2103	22.5872	3.3236	21.3495	2.2429	19.4634
318	8.1912	25.0224	5.2573	23.7380	3.5558	21.6664
356	13.1091	27.9332	8.2862	26.3951	5.6414	24.2120

Table 6. Comparison of the heat fluxes in three different samples at $x = 0.005$ m

Thickness (m)	Sample A		Sample B		Sample C	
	q^r (W/m^2)	q^c (W/m^2)	q^r (W/m^2)	q^c (W/m^2)	q^r (W/m^2)	q^c (W/m^2)
1.0	0.0525	0.2277	0.0333	0.2140	0.0224	0.1944
0.1	0.5249	2.2769	0.3331	2.4792	0.2241	1.9444
0.05	1.0493	4.5519	0.6662	4.2792	0.4481	3.8885
0.01	5.2103	22.5872	3.3236	21.3495	2.2429	19.4634

radiative heat flux by around 10.5% because the extinction coefficient is underestimated by using a constant value. The radiative heat flux for sample A is larger than sample C because the extinction coefficient of sample A is much smaller than sample C. Figure 5 depicts how evacuation pressure influences radiative conductivity, as defined by Eq. (6). As mentioned earlier, the radiative conductivities are nearly independent of evacuated pressure. For sample A, the radiative conductivity by diffusion method overestimated around 12% and the gray radiation overestimated around 7.6%, respectively.

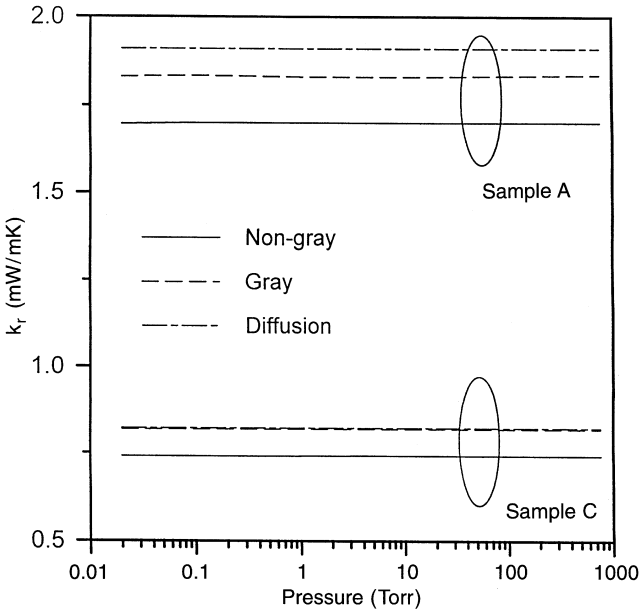

Fig. 5. Effects of evacuation pressure on radiative conductivity with $T_1 = 301$ K, $T_2 = 271$ K, $\varepsilon_1 = 0.1$, $\varepsilon_2 = 0.1$, and $L = 0.01$ m

Figure 6 presents how mean temperature influences radiative heat flux at an evacuation pressure of 0.02 Torr. The differences between sample A and sample C increase with an increase of mean temperature. However, the non-gray effects are only slight. Figure 7 displays the mean temperature on radiative conductivity. For higher temperatures, the radiative conductivity becomes even more prominent than the solid thermal conductivity. According to this figure, the profiles of gray radiation and diffusion methods tend to merge together with a decrease of the mean temperature. On the other hand, the profiles of gray and non-gray radiation methods tend to accumulate together with an increase of mean temperature. In sum, the relative error between the diffusion method and non-gray radiation method increases from 3% to 58% with a decrease of the mean temperature from 356 to 156 K. Therefore, the gray radiation and diffusion methods cannot accurately predict the radiative conductivity at a low mean temperature.

Figure 8 illustrates how thickness influences radiative heat flux at an evacuation pressure of 0.02 Torr. Apparently, the radiative heat flux calculated by gray method is approximately 10.4% larger than that by non-gray method for $L = 0.01$ m and 13.1% for $L = 0.05$ m. This observation is owing to that a larger thickness not only prevents the propagation of radiation emitting and scattering forward but also prevents the conductive heat transfer. Figure 9 depicts how thickness influences radiative conductivity. According to this figure, the radiative conductivity calculated by three methods is initially maintained constant with a decrease of the specimen's thickness. For sample A, the radiative conductivity calculated by diffusion method is around 9.4% larger than the non-gray method and 8% larger than by gray radiation, respectively.

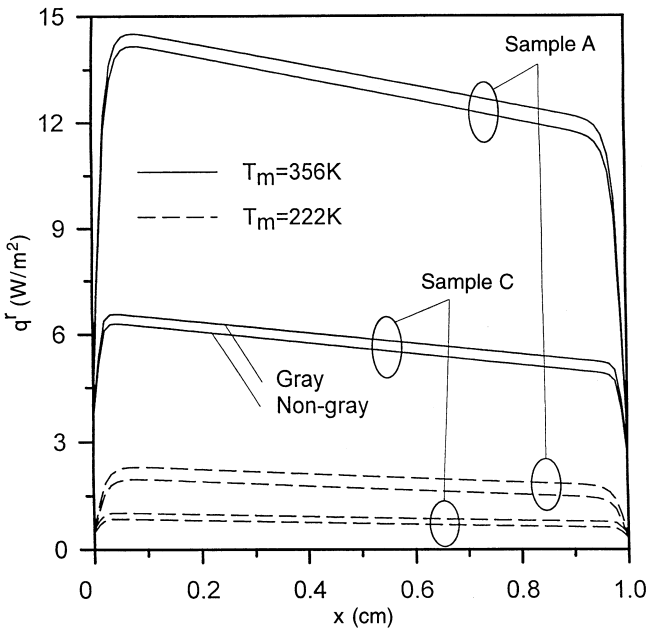

Fig. 6. Effects of mean temperature on radiative heat flux with $\varepsilon_1 = 0.1$, $\varepsilon_2 = 0.1$, $L = 0.01$ m, and an evacuation pressure of 0.02 Torr

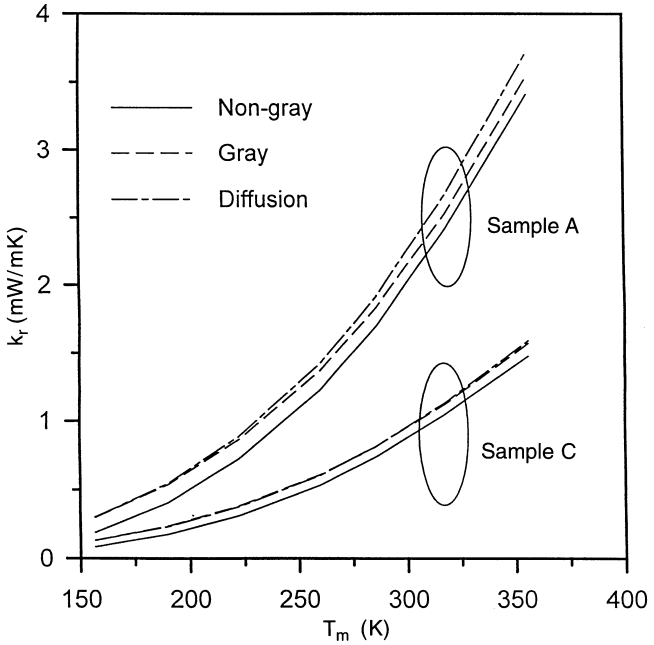

Fig. 7. Effects of mean temperature on radiative conductivity with $\varepsilon_1 = 0.1$, $\varepsilon_2 = 0.1$, $L = 0.01$ m, and an evacuation pressure of 0.02 Torr

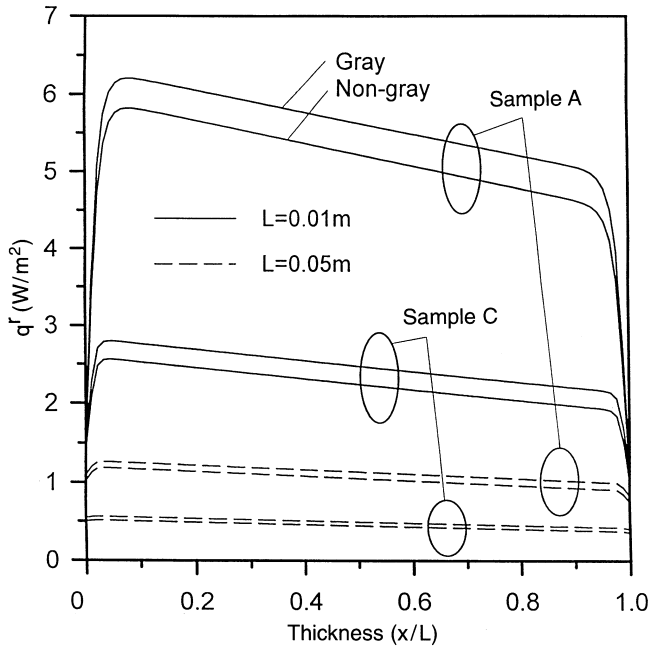

Fig. 8. Effects of media thickness on radiative heat flux with $T_1 = 301$ K, $T_2 = 271$ K, $\varepsilon_1 = 0.1$, $\varepsilon_2 = 0.1$, and an evacuation pressure of 0.02 Torr

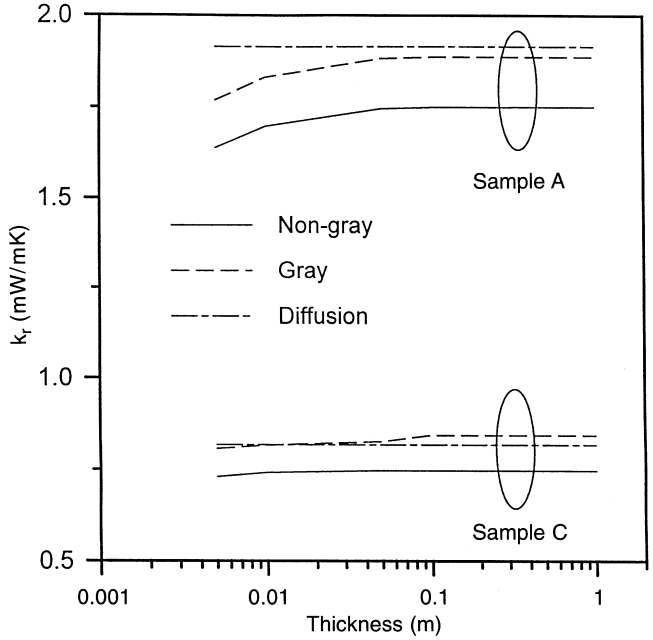

Fig. 9. Effects of media thickness on radiative conductivity with $T_1 = 301$ K, $T_2 = 271$ K, $\varepsilon_1 = 0.1$, $\varepsilon_2 = 0.1$, and an evacuation pressure of 0.02 Torr

Interestingly, a decrease of the specimen's thickness decreased to a critical value causes a decrease of the radiative conductivity. With a decrease of the specimen's thickness, the heat transfer mode is transformed from optical thick media to optical thin media. For the optical thin case, the conduction tends to be significant. Moreover, the radiative conductivity by diffusion method does not display the same tendency as the other two methods.

5 Conclusions

This study investigated the thermal performance of evacuated polyurethane foams with three different cell sizes. Samples were designed as 100% open cell rigid bodies. The box model was used to incorporate the characteristics of non-gray bands and coupled with the P-3 approximation method for calculating radiative heat transfer. The energy equation was solved using fully implicit finite-difference method. Experimental results indicated that solid and radiative contributions are independent of pressure, thereby allowing us to obtain gaseous conductivity at higher pressures by subtracting this measured result from the total heat transfer. In addition, the spectral extinction coefficient decreased with an increase of cell size; the radiative conductivity increased with an increase of cell size as well. Moreover, the radiative conductivity calculated by gray radiation method was around 8% higher than that by non-gray method, but nearly 58% higher in a low mean temperature case. On the other hand, the radiative conductivity calculated by diffusion method was approximately 17% higher than that by non-gray method for the optical thin case and 58% higher for the low mean temperature case.

References

1. **Aronson JR; Emslie AG; Ruccia FE; Smallman CR; Smith EM; Strong PF** (1979) Infrared emittance of fibrous materials. Appl Optics 18: 2622–2633
2. **Tong TW; Tien CL** (1980) Analytical models for thermal radiation in fibrous insulation. J Thermal Insulation 4: 27–43
3. **Tong TW; Tien CL** (1983) Radiative heat transfer in fibrous insulation – part I: analytical study. ASME J Heat Transfer 105: 70–75
4. **Tong TW; Yang QS; Tien CL** (1983) Radiative heat transfer in fibrous Insulation-part II: experimental study. ASME J Heat Transfer 105: 76–81
5. **Scheuerpflug P; Caps R; Buttner D; Fricke J** (1985) Apparent thermal conductivity of evacuated SiO_2-aerogel tiles under variation of radiative boundary condition. Int J Heat Mass Transfer 28: 2299–2306
6. **Chu HS; Stretton AJ; Tien CL** (1988) Radiative heat transfer in ultra-fine powder insulation. Int J Heat Mass Tranfer 31: 1627–1634
7. **Heinemann U; Caps R; Fricke J** (1996) Radiation-conduction interaction: an investigation on silica aerogels. Int J Heat Mass Transfer 39 (10): 2115–2130
8. **Glicksman LR; Schuetz M; Sinofsky M** (1987) Radiation heat transfer in foam insulation. Int J Heat Mass Transfer 30 (1): 187–197
9. **Kuhn J; Ebert HP; Arduini-Schuster MC; Buttner D; Fricke J** (1992) Thermal transport in polystyrene and polyurethane foam insulations. Int J Heat Mass Transfer 35 (7): 1795–1801
10. **Doermann D; Sacadura JF** (1996) Heat transfer in open cell foam insulation. ASME J Heat Transfer 118: 88–93
11. **Caps R; Heinemann U; Fricke J; Keller K** (1997) Thermal conductivity of polyimide foams. Int J Heat Mass Transfer 40 (2): 269–280
12. **Hahn O; Raether F; Arduini-Schuster MC; Fricke J** (1997) Transient coupled conductive/radiative heat transfer in absorbing, emitting and scattering media: application to laser-flash measurements on ceramic materials. Int J Heat Mass Transfer 40 (3): 689–698
13. **Tseng CJ; Yamaguchi M; Ohmori T** (1997) Thermal Conductivity of polyurethane foams from room temperature to 20 K. Crygenics 37: 305–312

14. **Modest MF** Radiative Heat Transfer. McGraw-Hill Inc. 1993
15. **Ratzel AC; Howell JR** (1982) Heat Transfer by conduction and radiation in one-dimensional planar media using the differential approximation. ASME J Heat Transfer 104: 388–391
16. **Özisik MN** Radiative transfer and interactions with conduction and convection. Wiley-Interscience, New York, 1973